Glucose-based surface modification of $Li_{1.2}Mn_{0.54}Ni_{0.13}Co_{0.13}O_2$ as a cathode material for lithium-ion batteries

Ke Li[1], Zewei Yuan[3], Haoran Yu[1], Kai Xia[1], Guodong Jiang[1,2], Jian Xiong[1,2], Songdong Yuan[1,2,]*

[1] Hubei Collaborative Innovation Center for High-efficiency Utilization of Solar Energy, Hubei University of Technology, Wuhan, 430068, China.
[2] The Synergistic Innovation Center of Catalysis Materials of Hubei Province, Wuhan 430068, China.
[3] Department of Chemistry, University of Amsterdam, Science Park904, 1098XH, Amsterdam, Netherlands
[*]E-mail: yuansongdong@aliyun.com

Under high voltage (> 4.4 V), many side reactions between the Li-rich Mn-based cathode materials and the electrolyte can occur, with a transition from the active lamellar phase to the inactive spinel phase occurring during cycling, which can reduce the cycle stability of the material. Glucose-based modification can significantly promote the electrochemical performance of $Li_{1.2}Mn_{0.54}Ni_{0.13}Co_{0.13}O_2$. After glucose-based modification, the sample surface after treatment confirmed the presence of chemically activated Li_2MnO_3 components and the $LiMn_2O_4$ spinel phases. Furthermore, the material capacity changed significantly at high rates. The 1 C discharge capacity of the raw material was 165.2 mAh/g, and the sample at 1 C discharge capacity after 10% glucose treatment was 183 mAh/g, while the capacity retention rate after 100 cycles was 98.5%. The initial coulombic efficiency of the sample after treatment increased from 71.3% for the raw material to 78.5%, and the impedance also significantly reduced. The significant improvement in electrochemical performance of the sample after treatment was attributed to the newly formed layered spinel surface and chemically activated Li_2MnO_3 phase, which significantly enhanced the redox reactions on the surface of the positive electrode, accelerating the diffusion rate of Li^+ and adjusting the electrochemical evolution behavior of the Li-rich layered oxides.

1. INTRODUCTION

The pursuit of higher specific capacity has been the unremitting goal of lithium-ion researchers. Systems that burn fossil energy to provide kinetic energy are still widely used in modern automobiles. However, the extensive use of fossil fuels has resulted in global warming and environmental pollution,

resulting mankind in higher requirements for the use of carbon emissions and other pollutants. Lithium (Li)- and manganese (Mn)-rich cathode materials have attracted the attention of numerous researchers due to their high specific capacity. Specifically, Li-rich layered cathode materials and Si/C composite anode materials are considered the most promising candidates for high energy density Li-ion batteries with long life spans. Li- and Mn-rich anode materials are denoted by xLi_2MnO_3 - $LiMO_2$ (1 - x)[1]. These materials have stable monoclinic Li_2MnO_3 layer structures, high specific capacities ($\geq$ 250 mAh/g), and have advantages such as a high degree of safety, a low cost, and a low production of pollution. However, they also have issues that restrict their commercial use, such as circulation capacity[2]、voltage decay, in poor performance[3, 4].

Spinel $LiMn_2O_4$ is an important Li-ion battery cathode material for multi-functional $LiMn_2O_4$ material structures with a complex phase diagram [5]. Research on the chemical properties and electrochemical performance of $LiMn_2O_4$ has led to the discovery and development of optimized high-pressure spinel cathode materials ($LiNi_{0.5}Mn_{1.5}O_4$) with high capacity layered rich Li-Mn based materials (such as Li_2MnO_3 and $xLiNi_{1/3}Co_{1/3}Mn_{1/3}O_2 \cdot (1-x)Li_2MnO_3$), as well as with other advanced cathode materials. However, although $LiMn_2O_4$ capacity and energy density than the later development of layered $LiNi_{1-x-y}Co_xMn_yO_2$ (NCM)[6], $LiNi_{1-x-y}Co_xAl_yO_2$ (NCA), Li- and Mn-rich cathode material[7-9] and $LiCoO_2$[10] cathode material smaller. Nevertheless, this material is cost-effective, non-toxic, and environmentally friendly, and also has fast diffusion dynamics. Furthermore, the stability of the crystal structure can be used to create layered cathode blends with reduced costs, increased structural and thermal stability, and improved rate performance[5, 11].

The low conductivity of Li_2MnO_3 components in Li- and Mn-rich cathode materials, along with their poor monoclinic phase ion transmission performance, causes slow Li^+ diffusion in the composite cathode material, resulting in the poor specific capacities of Li- and Mn-rich cathode materials. $LiMn_2O_4$ and $LiNi_{0.5}Mn_{1.5}O_4$ spinel phases are constructed on the surfaces of Li-rich Mn-based layered materials via chemical means in order to maximize the use of the three-dimensional Li insertion/extraction framework of the spinel structure, and the layered structure with a high Li storage capacity[12-15]. For example, Zhang[16] et al. designed and constructed a 10 nm thick $Li_xTM_{3-x}O_4$ spinel shell (TM = Ni, Co, Mn, 0 <x <1) on the material surface via electrochemical means, with both good structural stability of the TM_3O_4-type spinel phase and good Li^+ conductivity of the $LiMn_2O_4$-type spinel phase. The system structure and electrochemical analysis showed that it slowed down the activation rate of the Li_2MnO_3 component and effectively reduced the dissolution of Mn and the loss of O in the crystalline lattice under high pressure (> 4.5 V), thereby inhibiting the structural degradation of the material from the lamellar phase (active phase) to the spinel phase (inactive phase), significantly improving cycle stability. Glucose is the most common monosaccharide in nature and is renewable, environmentally friendly, inexpensive, and abundant. Under alkaline conditions, glucose has a certain degree of reduction. Therefore, in this work, we proposed a glucose-based surface modification method. The in-situ spinel phase and chemically activated Li_2MnO_3 phase formed on the surface of the modified sample, which improved the electrochemical performance of the $Li_{1.2}Mn_{0.54}Ni_{0.13}Co_{0.13}O_2$ material.

2. EXPERIMENTAL

2.1 Preparation of LRM

The precursor of $Mn_{0.54}Ni_{0.13}Co_{0.13}(CO_3)_{0.8}$ was synthesized using a co-precipitation method. The precursor and Li_2CO_3 (excess 5%) were mixed and ground at a mass ratio of 2:1.15, pre-fired at 500°C for 6 h, and then the pre-heated mixture was removed. A certain amount of molten salt was added (LiCl: NaCl=1: 3) to the mixture and ground, where the mass ratio of the precursor to the molten salt was 1:4. Then, the ground mixture was calcined at 900°C for 10 h to obtain $Li_{1.2}Mn_{0.54}Ni_{0.13}Co_{0.13}O_2$ (LRM).

2.2 Preparation of LRM@Spinel

First, 0.1 g of glucose was dissolved in 50 mL of deionized water, and 500 μL of ammonia (to improve the reducibility of glucose) was added into the mixture. Then, 2 g of the prepared LRM powder was added into the mixture at a 5% ratio of glucose to active substance, and the reactor was heated in a water bath at 90°C for 3 h, under conditions of heating and stirring. Then, the heated suspension was suction-filtered, the filtered solid was dried at 60°C for 12 h, and finally the dried solid was heated at 350°C for 3 h to obtain the final sample, which was labeled as LRM-1. In addition, samples with 10% and 15% ratios of glucose to active substance were marked as LRM-2 and LRM-3, respectively.

2.3 Electrode preparation

The LRM, LRM-1, LRM-2, and LRM-3 electrodes were prepared by mixing the active materials, carbon-black conductive additive (Super P), and polyvinylidene fluoride (PVDF) with a mass ratio of 8:1:1 in N-methyl-2-pyrrolidone (NMP), then rolled out on an aluminum foil surface. After vacuum-drying at 80°C for 12 h, the aluminum foil with the slurry was cut into an electrode with a 12 mm diameter. The load of the electrode was about 2.5 mg/cm^2. All electrodes were assembled into a 2032 type coin cell with a fiberglass separator and Li metal in an Ar-filled glovebox. Then, 100 μL of electrolyte solution was added to the separator, and 1 mol/L LiPF6 (EC + DMC + DEC) (volume ratio of EC, DMC, and DEC was 1:1:1) was used as the electrolyte. The charge-discharge tests and rate tests at different current densities were conducted between 2.0 and 4.8 V (versus Li$^+$/Li) on a battery test station (Arbin Instruments, USA). Cyclic voltammetry (CV) and electrochemical impedance spectroscopy (EIS) were performed with coin cells using the electrochemical workstation (Zahner Zennium, Germany). CV was conducted at a scan rate of 0.1 mV/s, with the voltage ranging from 2.0 V to 4.8 V, and EIS was performed with a 10 mV amplitude between 10 mHz and 100 kHz.

2.4 Characterization of the material

The morphologies of LRM, LRM-1, LRM-2, and LRM-3 were characterized by scanning electron microscopy (SEM, Hitachi SU-8010, Japan). The structures of LRM, LRM-1, LRM-2, and LRM-3 were recorded by X-ray diffraction (XRD, PANalytical B.V. Empyrean, Netherlands), with Cu kα radiation over a 2θ range of 10°–80°. The surface chemistry of LRM and LRM-2 were detected by X-ray photoelectron spectroscopy (XPS, Thermo Fisher). The phase structures of LRM and LRM-2 were measured by laser Raman spectroscopy (DXR), and the surface microstructure of LRM and LRM-2 were characterized by transmission electron microscopy (TEM).

3. RESULTS AND DISCUSSION
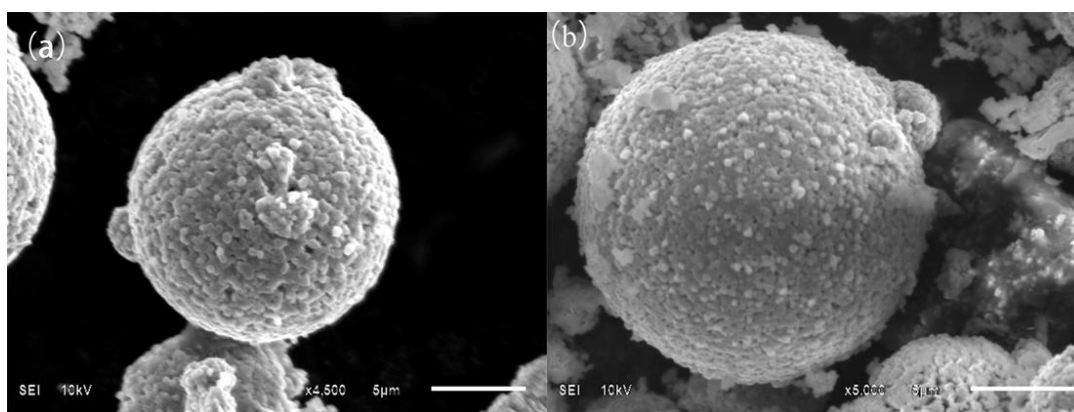
Figure 1. SEM of LRM (a) and LRM-2 (b).

Figure 1 shows the SEM image of LRM (a) and LRM-2 (b), indicating that the size of the secondary particles was about 10 μm, and the surface modification of glucose did not affect the particle size of the secondary particles. The primary particles changed slightly, and the shapes of the primary particles became sharp. These changes in material morphology were possibly caused by the formation of the spinel phase on the surfaces of the primary particles.

The effects of glucose modification on the phase structures of the Li- and Mn-rich cathode materials were detected by XRD. Figure 2 shows the XRD patterns of the LRM, LRM-1, LRM-2, and LRM-3 materials and the (101) peak partial increase of the material as obtained by XRD. The XRD structure diagram corresponded to the rhombic α-NaFeO$_2$ structure and the monoclinic Li$_2$MnO$_3$ phase. The peaks in the spectrum were obvious, strong, and sharp, without impurity peaks, indicating that the prepared LRM was pure with good crystallinity. The XRD diffraction pattern of the Li-rich Mn-based material after glucose treatment was the same as the Li-rich Mn-based raw material, indicating that glucose treatment did not affect the structures of the Li- and Mn-rich cathode materials. The (006)/(012) and (018)/(110) peaks in the XRD pattern of the Li- and Mn-rich cathode materials were obviously split, indicating that the synthesized Li- and Mn-rich cathode materials all had a stable layered structure[17]. The appearance of a weak diffraction peak near 2θ = 20.25° indicated the presence of the Li$_2$MnO$_3$ phase in the material[18]. Li$_2$MnO$_3$ belongs to the C2/m space group. Thus,

as shown in Figure 2 (b), the diffraction peak shifted to the large angle region as the glucose mass ratio increased, indicating that the unit cell volume of the modified sample contracted. Sample lattice volume shrinkage was attributed to the extraction of Li^+ and lattice oxygen from the Li_2MnO_3 phase during the glucose modification process[19].
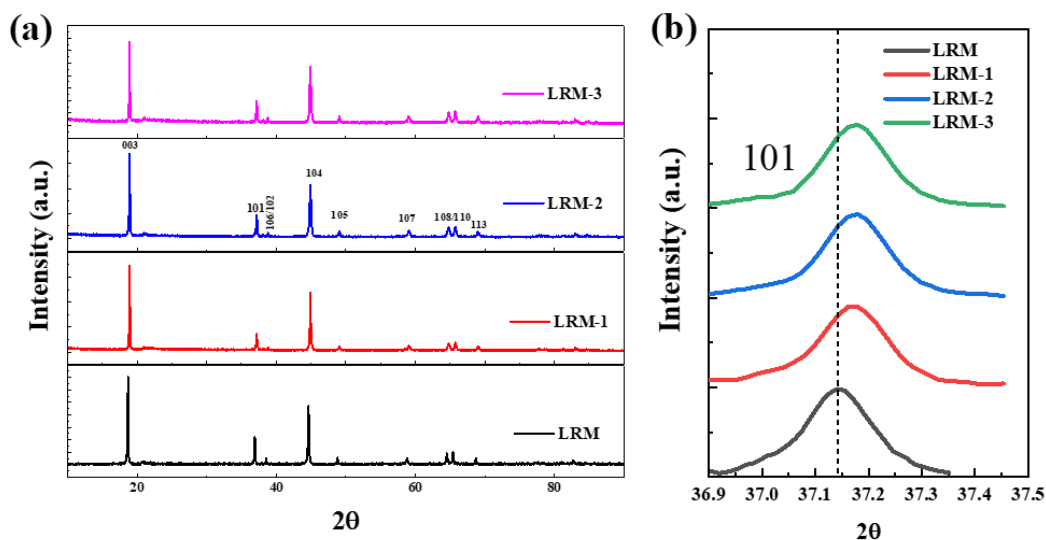

Figure 2. Full (a) and magnified (b) XRD patterns of LRM, LRM-1, LRM-2, and LRM-3.

To further explore the effects of glucose treatment on the surfaces of the Li- and Mn-rich cathode materials, XPS was used to detect surface chemical changes of LRM and LRM-2. As shown in Figure 3 (a), there was a significant difference between the surface elemental content of the sample after modification of the raw material. Mn concentration on the surface of the LRM-2 sample increased significantly after glucose treatment, indicating Mn enrichment on the sample surface after glucose treatment. Because the 2p binding energy of Mn split multiple times, it was difficult to accurately analyze the valence state of Mn; therefore, the spectrum of the $Mn2p_{3/2}$ peak was used for analysis. As shown in Figure 3 (d), the spectrum between 640 and 645 eV was the $Mn2p_{3/2}$ peak[20]. The $Mn2p_{3/2}$ peak of the Li-rich Mn-based raw material LRM was significantly smaller than the LRM-2 sample after glucose treatment. The Mn2p cracking peaks of Mn^{3+} and Mn^{4+} in LRM-2 were larger than the LRM, indicating that Mn^{3+} and Mn^{4+} content in the LRM-2 sample was higher after glucose treatment. We speculated that calcination after glucose treatment promoted the formation of the Mn-rich phase on the material surface, resulting in the enrichment of surface Mn and increased Mn^{3+} and Mn^{4+} content.
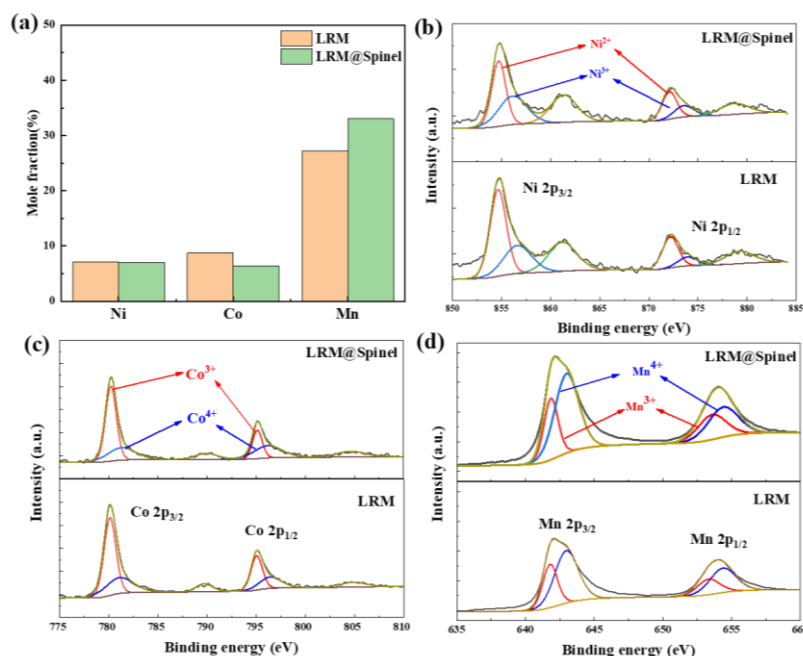
Figure 3. (a) Surface composition of LRM-2 as obtained from the XPS patterns of (b) Ni 2p, (c) Co 2p, (d) Mn 2p.
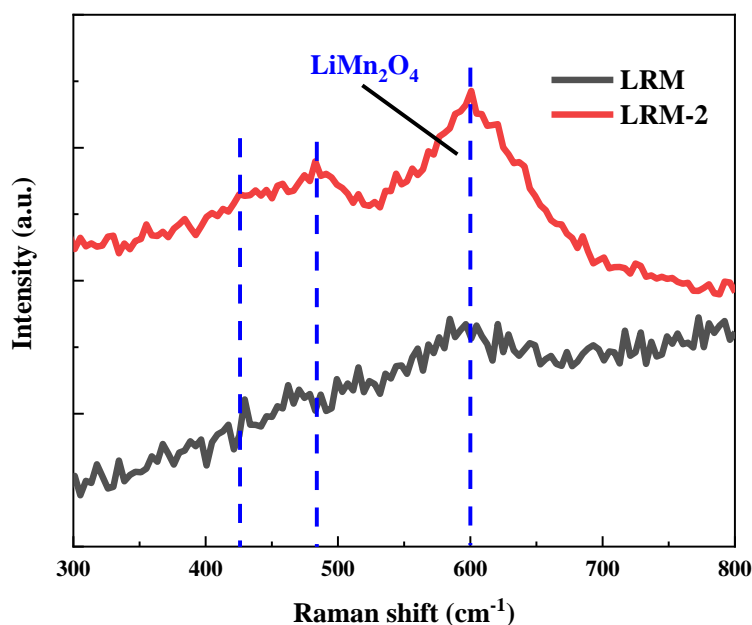

Figure 4. Raman patterns of LRM and LRM-2.

To explore the surface changes of the material after glucose modification, Raman spectroscopy was performed on the Li- and Mn-rich cathode raw material (LRM) and the glucose-modified material (LRM-2), and the results are shown in Figure 4. The figure shows that several Raman peaks appeared at 389, 426, 495, 600, and 636 cm^{-1} for the LMR-2 sample[21], and the relevant peaks were close to the Raman peaks of the spinel LiMn$_2$O$_4$. Due to the vibration of the Mn^{IV}-O bond, the presence of a shoulder near 600 cm^{-1} was considered to be the F$_{2g}^{(1)}$ mode, and the Raman bands near 495 and 426 cm^{-1} were assigned to the F$_{2g}^{(2)}$ and Eg modes, caused by Li-O vibrations of the LiO$_4$ group. Many

studies have shown that the intensity of the shoulder peak at 600 cm^{-1} is closely related to the average oxidation state of Mn in the spinel phase[21, 22]. In this work, we observed a weak peak for LRM at 600 cm^{-1}, which corresponded to the vibration of the Mn^{IV}-O bond, with no obvious peaks in the other bands, indicating that glucose treatment induced the formation of the LiMn$_2$O$_4$ spinel phase on the surfaces of the Li- and Mn-rich cathode materials.

Surface microstructure plays an important role in determining the Li-ion redox reaction in the Li-rich Mn-based layered oxide, and a sample microstructure after glucose surface modification was observed under high-resolution TEM. Figure 5 (a) shows the TEM image of the sample after glucose treatment, and Figure 5(b) shows the TEM image of the Li$_{1.2}$Mn$_{0.54}$Ni$_{0.13}$Co$_{0.13}$O$_2$ raw material. As shown in Figure 5 (b), the inter-plane spacing of 0.47 nm corresponded to the Li-rich phase, and inter-plane spacings of 0.41 and 0.28 nm are shown in Figure 5 (a). The 0.41 nm spacing was consistent with the (−111) plane of the Li$_2$MnO$_3$ monoclinic phase (JCPDS No.27-1252), and the 0.28 nm spacing was consistent with the (220) plane of the LiMn$_2$O$_4$ cubic spinel structure (JCPDS No.32-0782)[22]. The TEM characterization results were consistent with the XPS and Raman spectroscopy results. After glucose modification, the spinel phase was induced on the surface of the raw material, resulting in the enrichment of surface Mn.

After glucose modification, the inner layer of the sample layered core and outer layer of the spinel phase were in close contact. This phenomenon was caused by the diffusion of metal ions on both sides during heat treatment[23]. The diffusion of metal ions led to the integration of the spinel into the rich Li layered structure; therefore, the interface between the layered core and the outer spinel had good Li$^+$ penetration. Due to the structural compatibility of the cubic closed spinel LiNi$_x$Mn$_{2-x}$O$_4$ (0 < x ≤ 0.5) with Li-rich layered metal oxides[24], the composite material had high structural stability. In addition, the three-dimensional Li$^+$ diffusion channel of the spinel ensured rapid Li$^+$ exchange with the electrolyte. Compared to the surfaces of the LRM particles, the spinel phase formed in situ on the surfaces of the LRM-2 particles, endowing the processed samples with higher Li$^+$ conductivity and higher electronic conductivity, which was beneficial to the redox reactions on the positive electrode/electrolyte interface during the charging and discharging processes.
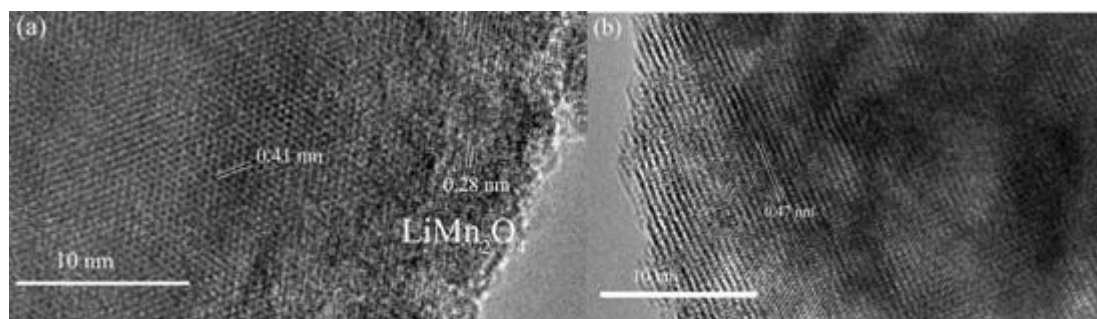

Figure 5. TEM images of LRM-2 (a) and LRM (b).

Figure 6 (a) shows the first-round charge-discharge curve of the material after glucose surface modification at 0.1 C (25 mA/g). The figure shows that the charge-discharge curve was divided into two sections, where one was from the open circuit voltage to 4.5 V, and the other was from 4.5 to 4.8

V, and this section was due to the movement of Li^+ from the inactive Li_2MnO_3 phase and the oxidation reaction of O elements, generating O_2[25, 26]. The initial coulombic efficiencies of LRM, LRM-1, LRM-2, and LRM-3 were 71.3%, 72.2%, 78.5%, 72%, respectively. Therefore, glucose modification improved the initial coulombic efficiency of the sample. The initial irreversible capacity was reduced to 71.1 mAh/g compared to the 94.9 mAh/g of the raw material, which was related to the introduction of the spinel phase and the activation of the Li_2MnO_3 phase. As the ratio of glucose to active material increased, the discharge voltage decreased significantly, indicating that glucose treatment could effectively change the discharge behaviors of the Li-rich Mn-based cathode materials. In addition, a weak discharge platform appeared in the first circle of the sample near 2.75 V in the discharge curve after glucose treatment, corresponding to the charge and discharge behavior of the spinel phase. Compared to the raw LRM material, the CV curves of LRM-1, LRM-2, and LRM-3 varied greatly, clearly proving that glucose can be used to effectively modify Li- and Mn-rich cathode materials to adjust the electrochemical behavior of Li-rich layered oxides. As shown in the figure, additional oxidation peaks (O_1) and reduction (R_1) peaks were observed in the CV curve of LRM-2, located at 2.97 and 2.75 V, respectively. These peaks corresponded to the release and embedment of Li^+ in the newly formed spinel phase $LiMn_2O_4$[27], which was consistent with the XPS, Raman, and TEM characterization results. Additional redox peaks (O_5/R_5) were also observed, as shown in the figure below, for the sample after glucose surface modification. The oxidation peak at 4.0 V was asymmetric, where the wider shoulder peak was due to the multi-step oxidation process of Ni ions, with corresponding R_2 and R_3 reduction peaks[28]. Therefore, the oxidation peak at 4.0 V may have been the combined effect of O_2, O_3, and O_5[29]. The R_5 peak was attributed to the reduction of Mn^{4+} in the MnO_2-rich domain, and Mn^{4+} was due to the oxidation of Mn^{3+} and Mn^{2+} ions in the chemically activated Li_2MnO_3 phase[30]. However, the O_5 peak was attributed to the extraction of Li^+ from the chemically activated Li_2MnO_3 phase in the first cycle, and to the extraction of Li^+ from Li_xMnO_2 in the subsequent cycle.

Figure 7 (a) shows the rate performance comparison of the raw material and the material after glucose treatment. The discharge capacities of the raw LRM material at 0.1 C and 1 C were 248.4 and 164.2 mAh/g, and the discharge capacities of LRM-2 are 256.2 and 181.3 mAh/g. The sample after glucose modification exhibited better rate performance, which was consistent with the CV results. In addition, the rate performance of the material after glucose treatment was significantly improved, due to the combined contributions of chemical activation of the Li_2MnO_3 phase, the exposure of more Li conductive surfaces, an increase in the specific surface area, and the in-situ formation of the spinel phase. Also, the cubic spinel structure had a good Li^+ transmission channel. The increase in specific surface area and the exposure of more Li conductive surfaces increased the contact area between the material and the electrolyte, which increased Li-ion insertion and the extraction rate. Therefore, the rate performance improved[31].
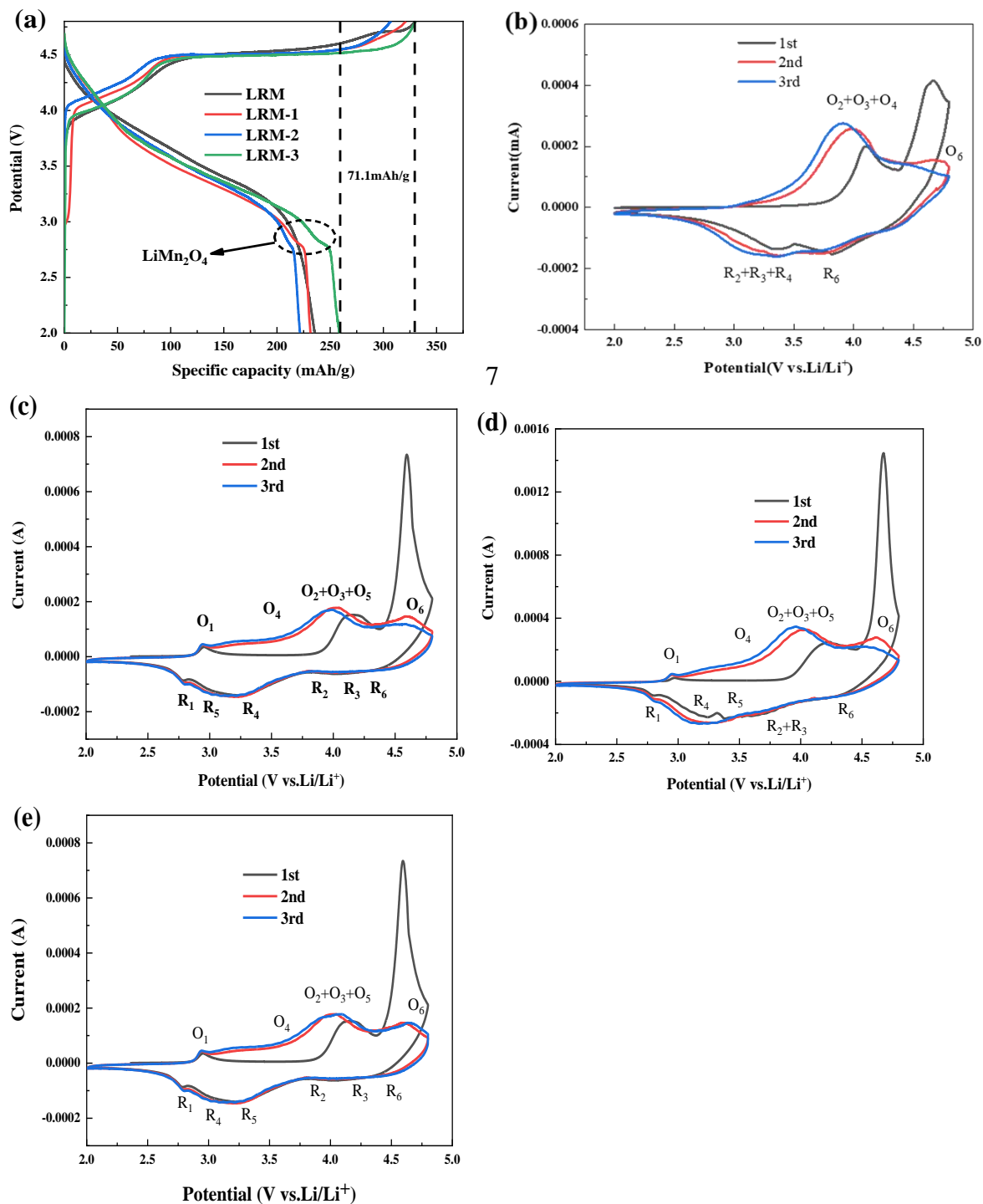
Figure 6. Initial charge-discharge curves (a) and CV curves of the samples: (b) LRM, (c) LRM-1, (d) LRM-2, and (e) LRM-3.

Figure 7 (b) shows the cycle performance results of the raw and glucose-modified materials. All batteries were activated at 0.1 C for three cycles and at 1 C cycle for 100 cycles. After 100 cycles, the capacity of LRM-1 was 162.9 mAh/g and the capacity of LRM-2 was 183 mAh/g. The sample with a glucose to raw material ratio of 10% had the best cycle performance. After 100 cycles at 1 C, the capacity retention rate after cycling was 98.5%. The beneficial spinel phase was introduced into the

Int. J. Electrochem. Sci., 17 **(2022)** Article Number: 220220

10

surface interface of the Li- and Mn-rich cathode materials to inhibit the transformation of the active to the inactive spinel phase in the material, separating the active component phase from the electrolyte. Thus, the beneficial spinel could play a role in protecting the active components, while reducing side reactions on the surface and the interface[22], thereby improving the cycle stability of the material.
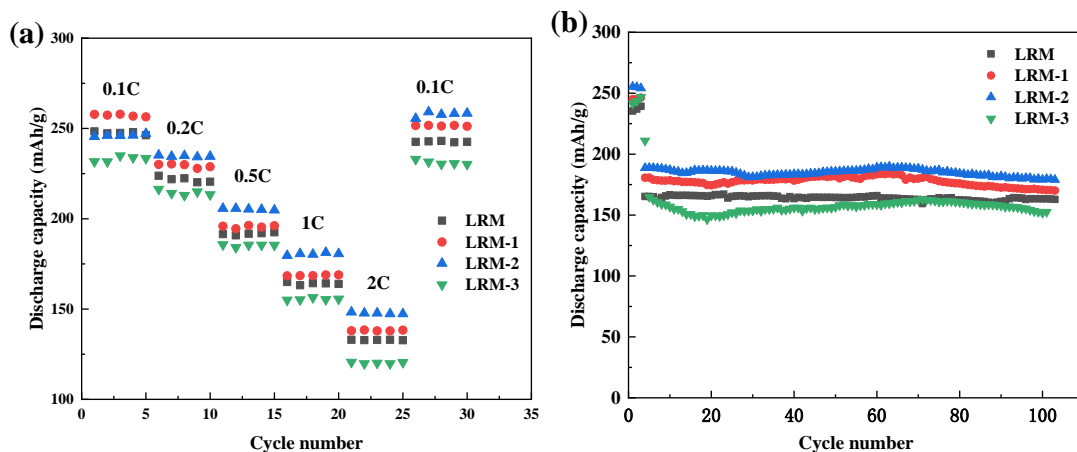

Figure 7. Specific capacity (a) and cycling performance (b) of LRM, LRM-1, LRM-2, and LRM-3.

Figure 8 (a) and (b) shows the charge and discharge curves of the raw LRM material and the LRM-2 glucose-modified sample at 1 C, with the charge and discharge curves of several typical cycles. As shown in the figure, the number of cycles increased, and both the raw and modified samples exhibited voltage attenuation, as shown by the arrow in the figure[32, 33]. However, voltage attenuation of the sample after glucose treatment was relatively small, indicating that glucose surface modification could suppress voltage attenuation.
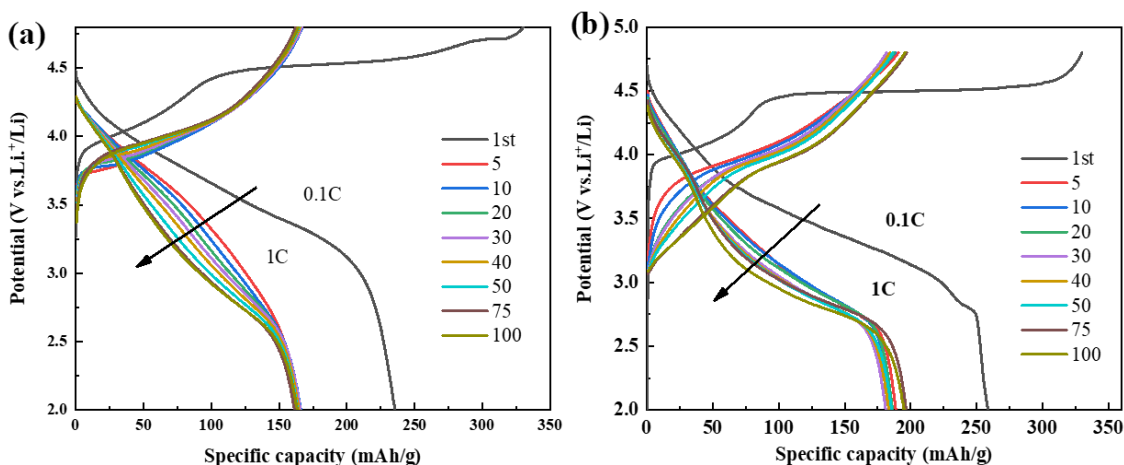
Figure 8. Charge-discharge curves of $Li_{1.2}Mn_{0.54}Ni_{0.13}Co_{0.13}O_2$: (a) LRM and (b) LRM-2.

To further explore the effects of glucose surface modification on the electrochemical performance of Li- and Mn-rich cathode materials, Nyquist plots were obtained for all samples that were not tested for charge and discharge capacities, and the test results are shown in Figure 9. The ohmic resistance related to Li-ion and electron transport was represented as a point on the AC impedance spectrum, as represented by resistance R_s.
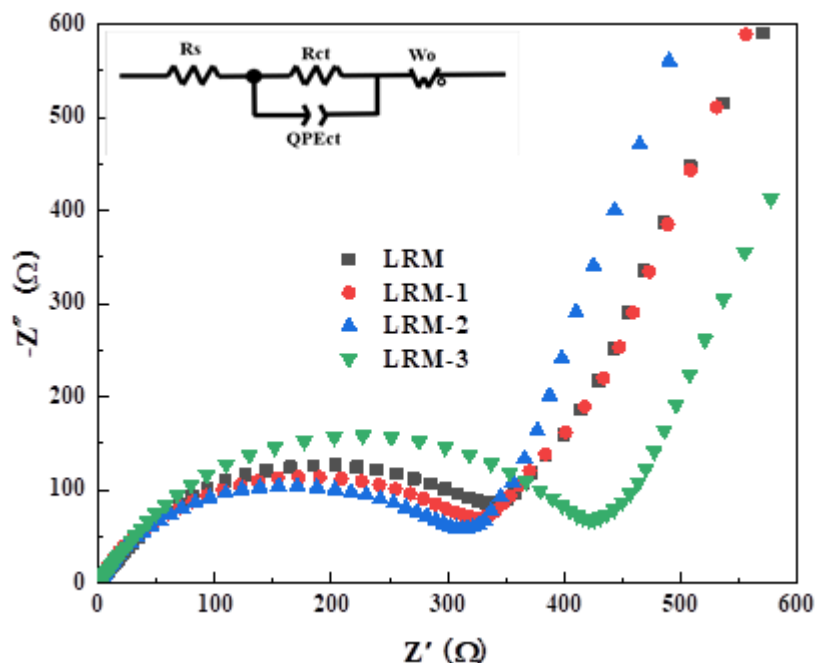
Figure 9. Nyquist plots acquired from the LRM, LRM-1, LRM-2, and LRM-3 based button cells.

The charge transfer resistance of Li^+ migration and diffusion through the surface insulator (SEI) of the active material was in the form of a semicircle on the Nyquist plots, which was represented by resistance R_{ct}. The oblique line in the low frequency region corresponded to the Warburg impedance, which affected the diffusion of Li-ions inside the material, as represented by Wo[34]. The calculated charge transfer impedance values of LRM, LRM-1, LRM-2, and LRM-3 were 340.1, 325.6, 312.4, and 421.2 Ω, respectively. The 10% sample had the lowest charge transfer resistance; therefore, Li^+ was quickly released from the surface of the material, which was consistent with the rate performance test results.

Table 1 shows a performance comparison of materials similar to Li-ion batteries. As shown in the table, the glucose-treated $Li_{1.2}Mn_{0.54}Ni_{0.13}Co_{0.13}O_2$ materials performed well at high rates, and they each had their own unique advantages compared to materials prepared via other methods.

Table 1. Performance comparison of similar materials

Author	Modification method	Conclusion
This work	Glucose-based surface modification $Li_{1.2}Mn_{0.54}Ni_{0.13}Co_{0.13}O_2$	The 1 C discharge capacity of the sample after 10% glucose treatment was 183 mAh/g, and the capacity retention rate was close to 98.5% after 100 cycles.
Song, Changkun[35]	TiO_2 coating	When the TiO_2 coating amount was equal to 1.0%, the first discharge-specific capacity reached 276.5 mAh/g at 0.1 C, and the Coulombic efficiency was also as high as 80.8%.
Li, Honglei[36]	Niobium doping	The discharge specific capacity was 265.8 mAh/g at 0.2 C with decelerated voltage decay, while 86.9% capacity remained after long-term cycling. Moreover, an excellent discharge specific capacity of 153.4 mAh/g was still attained at 5 C, accompanied by enhanced Li-ion diffusion kinetics.

4. CONCLUSIONS

The glucose-based modification method induced the formation of spinel $LiMn_2O_4$ and activated Li_2MnO_3 phases on the surface of Li-rich Mn-based materials through glucose modification, which promoted the electrochemical performance of Li-rich Mn-based layered oxides. Using XRD, SEM, XPS, TEM, constant current charge, discharge, CV, and EIS analysis, we studied the effects of glucose treatment on the phase structures, surface microstructures, and electrochemical performance of Li-rich layered oxides. As a result, chemically activated Li_2MnO_3 components and mixed $LiMn_2O_4$ spinel phases were confirmed on the treated sample surface; thus, glucose-based treatment could significantly promote the electrochemical performance of Li- and Mn-rich cathode materials. The 1 C discharge capacity of the raw material was 165.2 mAh/g and the capacity retention rate after 100 cycles was 98.4%, while the 1 C discharge capacity of the sample after 10% glucose treatment was 183 mAh/g and the capacity retention rate was close to 98.5% after 100 cycles. The performance of the material after glucose treatment was significantly improved in terms of rate performance, and the significant improvement in electrochemical performance of the modified sample was attributed to the introduction of the spinel phase and the chemical activation of the Li_2MnO_3 phase, which significantly enhanced the redox reaction on the surface of the positive electrode. This accelerated the Li diffusion rate and adjusted the electrochemical evolution behavior of the lithium-rich layered oxide.

COMPLIANCE WITH ETHICAL STANDARDS
Conflict of interest the authors declare that they have no conflict of interest.

References

1. P.K. Nayak, E.M. Erickson, F. Schipper, T.R. Penki, N. Munichandraiah, P. Adelhelm, H. Sclar, F. Amalraj, B. Markovsky and D. Aurbach, *Adv. Energy Mater.,* 8(2018)1702397.
2. X.Q. Yu, Y.C. Lyu, L. Gu, H.M. Wu, S.M. Bak, Y.N. Zhou, K. Amine, S.N. Ehrlich, H. Li, K.W. Nam and X.Q. Yang, *Adv. Energy Mater.*, 4(2014)1300950.
3. Y.K. Lei, J. Ni, Z.J. Hu, Z.W. Wang, F.K. Gui, B. Li, P.W. Ming, C.M. Zhang, Y. Elias, D. Aurbach and Q.F. Xiao, *Adv. Energy Mater.*, 10(2020)2002506.
4. A. Boulineau, L. Simonin, J.F. Colin, E. Canévet, L. Daniel and S. Patoux, *Chem. Mater.*, 24 (2012) 3558-3566.
5. Y.M. Huang, Y.H. Dong, S. Li, J. Lee, C. Wang, Z. Zhu, W.J. Xue, Y. Li and J. Li, *Adv. Energy Mater.,* 11(2020)2000997.
6. A. Manthiram, J.C. Knight, S.T. Myung, S.M. Oh and Y.K. Sun, *Adv. Energy Mater.*, 6(2016)1501010.
7. J.M. Zheng, S.J. Myeong, W.R. Cho, P.F. Yan, J. Xiao, C.M. Wang, J. Cho and J.G. Zhang, *Adv. Energy Mater.,* 7(2016)1601284.
8. H.L. Wu, X.H. Li, Z.X. Wang, H.J. Guo, W.J. Peng, Q.Y. Hu, G.C. Yan and J.X. Wang, *Electrochim. Acta*, 347 (2020)136279.
9. X.D. Zhang, J.L. Shi, J.Y. Liang, Y.X. Yin, J.N. Zhang, X.Q. Yu and Y.G. Guo, *Adv. Mater.*, 30(2018)1801751.
10. Y.C. Lyu, X. Wu, K. Wang, Z.J. Feng, T. Cheng, Y. Liu, M. Wang, R.M. Chen, L.M. Xu, J.J. Zhou, Y.H. Lu and B.K. Guo, *Adv. Energy Mater.*, 11(2020)2000982.
11. M.J. Young, S. Letourneau, R.E. Warburton, W.M. Dose, C. Johnson, J. Greeley and J.W. Elam, *The Journal of Physical Chemistry* C, 123(2019) 23783-23790.
12. F. Wu, N. Li, Y.F. Su, H.F. Shou, L.Y. Bao, W. Yang, L.J. Zhang, R. An and S. Chen, *Adv. Mater.*, 25(2013) 3722-6.
13. Q.B. Xia, X.F. Zhao, M.Q. Xu, Z.P. Ding, J.T. Liu, L.B. Chen, D.G. Ivey and W.F. Wei, *J. Mater. Chem.* A, 3(2015) 3995-4003.
14. D. Luo, S.H. Fang, L. Yang and S.I. Hirano, *ChemSusChem*, 10(2017) 4845-4850.
15. D. Gao, Z.S. Zeng, H.W. Mi, L.N. Sun, X.Z. Ren, P.X. Zhang and Y.L. Li, *J. Mater. Chem.* A, 9 (2021) 10508.
16. M.J. Zhang, Z.B. Li, L. Yu, D.F. Kong, Y.W. Li, B. Cao, W.G. Zhao, J.G. Wen and F. Pan, *Nano Energy*, 77 (2020)105188.
17. L. Ku, Y.X. Cai, Y.T. Ma, H.F. Zheng, P.F. Liu, Z.S. Qiao, Q.S. Xie, L.S. Wang and D.L. Peng, *Chem. Eng. J.,* 370 (2019) 499-507.
18. J. Li, R. Klöpsch, M.C. Stan, S. Nowak, M. Kunze, M. Winter and S. Passerini, *J. Power Sources*, 196 (2011) 4821-4825.
19. K.J. Xu, S.L. Pang, Y.G. Wang, X.Q. Shen, H.R. Wen, W.Z. Wang, Y.J. Su and X.M. Xi, J. *Electrochem. Soc*., 164(2017) A2348-A2354.
20. Z.Y. Luo, Z.W. Zhou, Z.J. He, Z.M. Sun, J.C. Zheng and Y.J. Li, *Ceram. Int*., 47(2021) 2656-2664.
21. B.B. Sahu, S.H. Kim, S. Kim, J.G. Han and S. Kim, *Surf. Coat. Technol*., 397 (2020)126066.
22. Y.L. Ding, J.A. Xie, G.S. Cao, T.J. Zhu, H.M. Yu and X.B. Zhao, *Adv. Funct. Mater*., 21(2011)

348-355.
23. Y.K. Sun, D.H. Kim, C.S. Yoon, S.T. Myung, J. Prakash and K. Amine, *Adv. Funct. Mater*., 20(2010) 485-491.
24. M.M. Thackeray, S.H. Kang, C.S. Johnson, J.T. Vaughey, R. Benedek and S.A. Hackney, *J. Mater. Chem.,* 17(2007)3112-3125.
25. S.L. Cui, Y.Y. Wang, S. Liu, G.R. Li and X.P. Gao, *Electrochim. Acta*, 328 (2019)135109.
26. J. Hong, H. Gwon, S.K. Jung, K. Ku and K. Kang, *J. Electrochem. Soc*., 162(2015) A2447-A2467.
27. S.L. Pang, M. Zhu, K.J. Xu, X.Q. Shen, H.R. Wen, Y.J. Su, G.M. Yang, X. Wu, S.W. Li, W.Z. Wang, X.M. Xi and H.B. Wang, *J. Electrochem. Soc*., 165(2018) A1897-A1902.
28. K. Kleiner, B. Strehle, A.R. Baker, S.J. Day, C.C. Tang, I. Buchberger, F.F. Chesneau, H.A. Gasteiger and M. Piana, *Chem. Mater*., 30(2018) 3656-3667.
29. Y.F. Chen, K. Xie, C.M. Zheng, Z.Y. Ma and Z.X. Chen, *ACS Appl. Mater. Interfaces*, 6(2014) 16888-94.
30. H.J. Yu, H.J. Kim, Y.R. Wang, P. He, D. Asakura, Y. Nakamura and H.S. Zhou, *Phys. Chem. Chem. Phys.,* 14(2012) 6584-95.
31. S.L. Pang, K.J. Xu, Y.G. Wang, X.Q. Shen, W.Z. Wang, Y.J. Su, M. Zhu and X.M. Xi, *J. Power Sources,* 365 (2017) 68-75.
32. J. Liu, Q.M. Liu, H.L. Zhu, F. Lin, Y. Ji, B.J. Li, J.F. Duan, L.J. Li and Z.Y. Chen, *Materials* (Basel), 13(2020)0040.
33. M. Sathiya, A.M. Abakumov, D. Foix, G. Rousse, K. Ramesha, M. Saubanere, M.L. Doublet, H. Vezin, C.P. Laisa, A.S. Prakash, D. Gonbeau, G. VanTendeloo and J.M. Tarascon, *Nat. Mater*., 14 (2015) 230-8.
34. D. Liu, F.Y. Wang, G. Wang, C.J. Lv, Z.Y. Wang, X.C. Duan and X. Li, *Molecules* , 24(2019)1680.
35. C.K. Song, W.J. Feng, Z.J. Shi and Z.Y. Huang, *Ionics*, 27(2021)457-468.
36. H.L. Li, Z.X. Jian, P.H. Yang, J.J. Li, Y.L. Xing and S.C. Zhang, *Ceram. Int*., 46(2020)23773-79.